Derivation of an Observation-Based Map of North African Dust Emission

Amato T. Evan*[1], Stephanie Fiedler[2], Chun Zhao[3], Laurent Menut[4], Kerstin Schepanski[5], Cyrille Flamant[6], Owen Doherty[1]

[1]Scripps Institution of Oceanography, University of California San Diego, La Jolla, California, USA.
[2]School of Earth and Environment, University of Leeds, LS2 9JT Leeds, UK, now at Karlsruhe Institute of Technology, 76131 Karlsruhe, Germany
[3]Atmospheric Sciences and Global Change Division, Pacific Northwest National Laboratory, Richland, WA, USA
[4]Institut P.-S. Laplace, Laboratoire de Météorologie Dynamique, CNRS UMR 8539, Ecole Polytechnique, Palaiseau, France.
[5]Leibniz Institute for Tropospheric Research, Leipzig, Germany
[6]Laboratoire Atmosphère, Milieux, Observations Spatiales, UMR 8190, CNRS, Sorbonne Université, UPMC and UVSQ, Paris, France..

* Correspondence to: Amato Evan (aevan@ucsd.edu)

Revision to: *Aeolian Research*

Abstract

Changes in the emission, transport and deposition of aeolian dust have profound effects on regional climate, so that characterizing the lifecycle of dust in observations and improving the representation of dust in global climate models is necessary. A fundamental aspect of characterizing the dust cycle is quantifying surface dust fluxes, yet no spatially explicit estimates of this flux exist for the World's major source regions. Here we present a novel technique for creating a map of the annual mean emitted dust flux for North Africa based on retrievals of dust storm frequency from the Meteosat Second Generation Spinning Enhanced Visible and InfraRed Imager (SEVIRI) and the relationship between dust storm frequency and emitted mass flux derived from the output of five models that simulate dust. Our results suggest that 64(±16)% of all dust emitted from North Africa is from the Bodélé depression, and that 13(±3)% of the North African dust flux is from a depression lying in the lee of the Aïr and Hoggar Mountains, making this area the second most important region of emission within North Africa.

1. Introduction

By mass, aeolian dust is the most pervasive aerosol on the planet, and the largest fraction of all global dust emission is in North Africa (e.g. Engelstaedter et al. 2006, Ginoux et al, 2006). African dust emission and transport is both affected by—and affects—the climate. For example, previous work has shown there is an increase in dust emission and transport over the Atlantic during periods of Sahelian drought (Prospero and Lamb, 2003) due to a decrease in soil moisture over the Sahel (Cowie et al. 2013), increased surface wind speeds over the Sahara (Ridley et al. 2014), or some combination of the two (Doherty et al. 2014). Once transported over the Atlantic, direct radiative forcing by dust both warms the atmosphere and cools the surface (Evan and Mukhopadhyay 2010), contributing interannual to decadal scale variability of tropical Atlantic sea surface temperatures (Evan et al. 2012) and exciting coupled modes of equatorial variability (Evan et al. 2011).

The influence of these aerosols on the climate system extends well beyond the direct radiative effect. Recent work has shown that African dust may influence clouds as far away as the west coast of the United States, providing ice nuclei required for precipitation in so-called atmospheric rivers (Creamean et al. 2013). Aeolian dust contains nitrogen, phosphorus and iron, all of which are required for primary productivity in oceanic and terrestrial ecosystems, and there is a large body of work demonstrating the importance of the atmospheric input of these elements via dust transported from western Africa (Das et al. 2013; Okin et al. 2011; Mahowald et al. 2010).

In order to improve understanding of dust-climate effects it is necessary to elucidate surface and atmospheric processes governing emission. However, the vast majority of North African dust emission occurs within largely uninhabited regions and thus there is a paucity of both meteorological and surface observations in these locations, particularly homogeneous measurements of each that span time scales of years to decades. As a result, numerical models play a crucial role in this field of study, yet there are relatively few observational data sets against which model output can be validated, and as a result model output is often validated against surface visibility observations and retrievals of aerosol optical depth from satellites and ground-based instrumentation—none of which are direct measures of dust—and surface concentrations from a limited number of sampling stations (*e.g.*, Ginoux et al, 2001, Huneeus et al, 2011; Tegen and Miller, 1998; Todd et al., 2008).

Given the lack of observations it is not surprising that recent studies have identified issues with the representation of the dust cycle in models. Kok (2011) evaluated the emitted size distribution of dust within several climate models, finding that all of the models underestimated the number of large particles emitted and thus the emitted mass flux, in agreement with earlier findings by Cakmur et al. (2006). Evan et al. (2014) examined dust in Climate Model Intercomparison Project Phase 5 (CMIP5) models, corroborating the findings of Kok (2011) and finding that, when forced by observed sea surface temperatures, models cannot reproduce historical year-to-year variability in cross-Atlantic dust transport, as determined by satellite data and paleo-proxy data. Furthermore, considering soil characteristics, Kok (2014) found

that a majority of models underestimate dust emissions sensitivity to the soil erodability, *i.e.* the ability of the soil to emit dust for a given above-threshold friction velocity (definition following Kok et al. 2014; Zender et al. 2003).

In the present paper we attempt to address the need for more observational records against which models can be evaluated by creating a spatially explicit map of annual dust emission using data from the Meteosat Second Generation Spinning Enhanced Visible and InfraRed Imager (SEVIRI). The remainder of this paper is organized as follows. In Section 2 we describe the models and satellite data used in this study. In Section 3 we compare the spatial structure of emission amount and emission frequency among the models, and define a statistical relationship between the two. In Section 4 we use this statistical relationship to derive the new observational climatology of dust emission amounts. We conclude in Section 5 with a summary of the main results of the paper.

2. Models and Satellite Data

In this paper we examine dust emission amount and frequency of events using one year of output from four regional models centered over North Africa and one global climate model. A summary of the models considered here and some of their relevant features can be found in Table 1.

2.1 Satellite Data

15-minute IR dust index images calculated from brightness temperatures at 8.7μm, 10.8μm and 12.0μm observed by SEVIRI MSG satellite are used inferring dust source activation frequencies over North Africa for the period March 2006 to February 2010 (Schepanski et al., 2007, 2012). As the images are available throughout day and night, dust source activation events were identified at sub-daily (hourly) resolution and geo-located by tracking back dust plumes individually to their point of origin, which is assumed to be the dust source and recorded on a 1°x1° map. It is noted that no dust sources can be spotted under optical thick clouds or dust plumes. Due to the 15-minute resolution of the native dust index images information on the diurnal cycle of dust source activation events can be retrieved, allowing for a relatively precise location of dust sources (Schepanski et al., 2012). Compared to an automated detection of dust plumes (Ashpole & Washington 2013), the manual identification by Schepanski et al. (2009) is likely less prone to systematic errors. Furthermore, the results from Ashpole & Washington do not cover all of North Africa, which is required for this study. The Schepanski et al. data set has been used for mapping dust sources (Schepanski et al., 2007), identifying the diurnal cycle of dust emission onset over Western Africa and associated meteorological conditions driving dust uplift (Schepanski et al., 2009), and model validation (e.g., Johnson et al., 2011). The dust source activation data set compares well with the spatio-temporal distribution of dust sources identified from surface visibility observations at weather stations (Laurent et al., 2010).

2.2 Models

In this study we examine the output from two dust simulations (Zhao et al. 2010; 2013) made with the Weather Research and Forecasting with Chemistry (WRF-

Chem) model (Grell et al. 2005; Skamarock et al. 2008). WRF-Chem simulates trace gases and particulates with the meteorological fields and simulates a variety of coupled physical and chemical processes such as transport, deposition, emission, chemical transformation, and radiation, and includes online coupling of chemistry and meteorology. WRF-Chem has been widely used to simulate the dust life cycle and climatic impact at the global scale (*e.g.*, Zhao et al., 2013) and the regional scale over West Africa (Zhao et al., 2010, 2011), Saudi Arabia (Kalenderski et al., 2013), North America (Zhao et al., 2012), and East Asia (Chen et al., 2013). The simulations are conducted at one-degree horizontal resolution throughout the domain. Two dust emission schemes, one based on Ginoux et al. (2001) and the other on Kok et al. (2014), both coupled with a modal aerosol model, are used in this study. The emission scheme from Ginoux et al. (2001) (hereafter referred to as WRF-GOCART) calculates the dust emission flux as a function of horizontal wind speed at 10 m, the threshold 10 m wind speed below which dust emission does not occur, and a prescribed source function that defines the potential dust source regions and comprises surface factors, such as vegetation and snow cover. The dust emission scheme developed by Kok et al. (2014) (hereafter referred to as WRF-KOK) is derived from a physically based theory that uses the concept that dust emission is a threshold effect without an explicitly prescribed dust source function. This parameterization depends only on the wind friction speed, the threshold friction speed, and the soil clay content.

We use output from the regional CHIMERE chemistry transport model. In CHIMERE dust emission is calculated following Alfaro and Gomes (2011) and Menut et al. (2005). The surface and soil properties are provided by USGS and STATSGO-FAO global databases, the aeolian roughness lengths are derived from ERS satellite data, as described in Menut et al. (2013). The wind speed is calculated using the WRFV3 regional model, forced by the NCEP global meteorological fields. All these data are projected onto a regular 1x1 degrees grid. In order to take into account the subgrid scale variability, a Weibull distribution is applied to the mean wind speed.

We also use output from the dust emission model of Tegen et al. (2002) following the setup of Fiedler et al. (2013a; 2014). Model dust emission is forced by 3-hourly wind speeds and soil moisture from ERA-Interim forecasts (Dee et al. 2011). The horizontal resolution of the model is 1° throughout the domain. In this model, hereafter referred to as TEGEN, a grid box is a potential dust source when at least two dust source activation events have been observed by SEVIRI satellite imagery between March 2006 and February 2010 (Schepanski et al. 2007; 2012).

In addition to these regional simulations, we examine dust emission from the global Community Earth System Model (Hurrell et al. 2013) with prescribed SST (hereafter referred to as CESM). Dust emission in CESM is based on the Dust Entrainment And Deposition (DEAD) model (Zender et al. 2003, Mahowald et al. 2006), modified to include saltation (Albani et al. 2014), as suggested by Kok 2011. In this experiment CESM is run at a resolution of 0.94° x 1.24° globally, using fixed (AMIP) SST and climatological land and surface properties. Here SSTs were prescribed from the

1982 season, although there was little difference in the results of this analysis using simulations forced with SSTs from two other years.

In CESM dust emission is calculated within the land model, the Community Land Model (CLM), and then passed to the atmospheric model, the Community Atmospheric Model (CAM). However, once passed to CAM the emission fluxes are scaled by a so-called "source function," which is a non-dimensional global map of soil erodibility from Zender et al. (2003). Emission fluxes from CESM are actually the scaled CAM fluxes. In this paper we examine both the CESM/CAM fluxes and the CLM fluxes.

In Table 1 is a summary of the salient features of the different models examined in this paper.

2.3 Intercomparison

For all models we firstly scaled emission fluxes so that the annual total emission from North Africa was equal to 4500 Tg, which is an observation-based estimate of annual North African dust emission (Evan et al. 2014). We next calculated the number of dust emission events in the models, where an event is defined as a 3-hourly dust emission flux greater than or equal to 1 $\mu g\ m^{-2}\ s^{-1}$ (Laurent et al. 2010; Tegen et al. 2013). We note that emission data from the CESM model is 3-hourly averaged, whereas from the WRF, ECHAM and CHIMERE models this is an instantaneous field. The emission frequency is defined as the total number of events divided by the total number of 3-hourly time-steps in the model output. Small changes in the threshold for detecting an event had no effect on the results from this study. This is because the total mass flux is dominated by regions that are frequently emitting at rates well above this threshold, and thus for our statistical analysis we disregard regions with low emission frequencies, as is discussed further in Section 3.3. In addition, we repeated the analysis after scaling emission fluxes from the models so that the annual total North African emission was from 500-4500 Tg, in increments of 500 Tg, finding qualitatively identical results in all cases, also discussed in Section 3.3.

3. Results

We first examine differences in annual dust emission and mean emission frequency among the models (Sections 3.1 and 3.2), we then use these data to identify a functional relationship between the two (Section 3.3).

3.1 Dust Emission Frequency

We compare the spatial structure of dust emission frequency in the models and from SEVIRI (Fig 1). Of the six data sets examined, WRF-GOCART and CHIMERE have the highest average dust emission frequencies, and the CHIMERE and CESM models exhibit the least spatial uniformity in these frequencies (*i.e.*, the standard deviation of the maps in Figure 1 are larger that that of the other three models). Since emissions are tuned to be equivalent amongst the models, on average WRF-GOCART and CHIMERE emit less dust per emission event than do the other models. Interestingly, WRF-KOK and WRF-GOCART are forced with identical wind fields

(Table 1) and thus lack of agreement between them is due to differences in the dust emission schemes. All the models except CESM and CLM show a maximum in emission frequency in the Bodélé depression (approximately between 15°-20°E and 15°-20°N). CHIMERE shows an additional peak in emission at the same latitude of the Bodélé but near the Atlantic coast. TEGEN, the WRF models and CLM show peaks in emission along the western coast between 20°-30°N and in the area of 0°E and 30°N. None of the models produce dust between 8°N and 12°N. Beyond these highly active regions, all models agree that there are other active regions to the east of the Bodélé and within Northern Africa (near the Mediterranean coast). The emission frequency maps for CESM and CLM show far less spatial structure than do the other models.

The map of annual mean dust emission frequency from SEVIRI shows a distinct band spanning approximately 15°-25°N, also with a regional maximum over the Bodélé depression, but a secondary maxima immediately to the west of the Bodélé (0°-10°W, which is in the Lee of the Aïr and Hoggar Mountains), which has been previously identified as an important dust source region (Kocha et al. 2013). Like the models SEVIRI does not show dust emission south of 12°N. We note that emission here likely occurs during the summertime in association with monsoon generated cold pools (Knippertz and Todd 2012). It is possible that these events are missed in the models due to lack of sufficient resolution to resolve such features, and in SEVIRI because these emission events are obscured under clouds. Qualitatively, the CHIMERE model exhibits the similarity to the spatial structure of the SEVIRI emission frequency map, although the magnitudes of the frequencies in SEVIRI are much smaller than those from CHIMERE, and are more similar to the WRF-KOK and TEGEN models. See Schepanski et al. (2009) for a detailed analysis of the spatial structure of the SEVIRI map of dust emission frequency.

Model differences in the spatial structures of emission frequency can also be elucidated by plots of the cumulative distribution functions (CDFs) of the annual mean dust emission frequency for each model. In order to facilitate intra-model comparison we linearly scaled the emission frequency for each model so that the maximum emission frequency is one. Only locations with a non-zero annual emission are included in the CDF calculations. The CDFs of the satellite data (SEVIRI), TEGEN, CHIMERE, WRF-KOK and CLM have an approximately logarithmic shape (Fig 2a), indicative of a small number of highly active regions (ref Fig 1). All of these models have CDF values greater than 80% at emission frequencies of 0.5 and above, meaning that 20% of the dust-emitting land areas have emission events more than 50% of the time. In contrast, the CDFs of WRF-GOCART and CESM increase slowly for small emission frequencies and then much more rapidly at high emission frequencies (Fig. 2a), reflecting a large number of locations that emit dust very frequently (compare Fig 1). Thus, for WRF-GOCART approximately 80% of the dust-emitting land surface areas have emission events more than 50% of the time.

As there is no regional network of surface observations of emission frequency it is not possible to determine which of the CDFs in Figure 2a are more realistic, and the SEVIRI data can not be used conclusively as a validation data set since it possibly

underestimates emission frequency along coast of West Africa and within the Saharan Heat Low region (Brindley et al, 2012). However, previous work has suggested that frequency maps should be characterized by a small number of highly active dust emission "hotspots" (Prospero et al. 2002; Engelstaedter and Washington 2006; Ginoux et al. 2012; Schepanski et al. 2012), and thus the SEVIRI data and those models exhibiting CDFs with a logarithmic shape (WRF-KOK, TEGEN, CHIMERE) may be more accurate than those with CDFs with cumulative frequencies that increase gradually for small emission frequencies (WRF-GOCART, CESM). We again note that we have scaled the models' annual cumulative North African dust emission to 4,500 Tg. However, we repeated the analysis after scaling the output to 1,000 Tg, obtaining similar results and identical conclusions about the model differences and agreement with SEVIRI.

3.2 Emitted Mass Flux

We next examine intra-model differences in the spatial structures of annual dust emission rates. For the purpose of an intra-model comparison of emission the value of the scaling factor has no effect on the results and their interpretation. All but the CESM model (Fig 3) show the Bodélé depression as having the highest annual emission rates within North Africa, which range from 1,200 (WRF-GOCART) to 7,000 (CHIMERE) g m^{-2} (Fig 3). WRF-KOK has two additional locations where emission is comparable to that of the Bodélé, in the lee of the Atlas Mountains (32°N & 5°W) and along the southernmost stretch of the western coast of the Red Sea (17°N & 37°E). In WRF-GOCART the region spanning 25°-30°N and 0°E and westward to the coastline, nominally characterized by the Saharan Heat Low during summer (Lavaysse et al. 2009), has an annual emission rate that is similar in magnitude to the Bodélé. The TEGEN and both WRF models show northeast Libya (30°N & 20°E) as being a region of high emission, but having annual emission rates that are still smaller than those for the Bodélé. We again note that differences in emission in the WRF models are due to dust emission schemes since the wind fields in each are identical.

Uniquely, the CESM model has an emission maximum in northeast Libya (30°N & 20°E), where the annual emission of approximately 4,000 g m^{-2} is nearly twice the value the model has within the Bodélé. In CLM there are local maxima in emission near the Northern Africa coast east of 10°E, but the regional maximum in emission is along the West African coastline between 25° and 30°N, and emission within the Bodélé is only a local maximum but is still far smaller than emission in the model hotspots to the north and west. Thus, while application of the source function in CESM produces a suspect dust maximum along the northern African coastline, it also increases the amount of dust emitted from the Bodélé, bring the CESM more in-line with the other models. It is interesting to note that the pattern of emission from CLM in the northwestern sector of the domain is very similar to the emission pattern from TEGEN, and that application of the source function moves this coastal emission further inland, which is more similar to the output from WRF-GOCART.

We also calculated CDFs of the models' annual emission (Fig 3). The emission CDFs (Fig 2b) exhibit greater intermodel agreement than do the CDFs of event frequency

(Fig 2a). The models' emission CDFs all have a logarithmic shape, indicating a small number of regions that dominate the total mass flux off of North Africa. Only WRF-GOCART shows a slightly distinct emission CDF, with a more gradual increase in the cumulative frequency than the other models. For example, for WRF-GOCART emission from 40% of the land surface area contributes 80% of the total dust flux, whereas for all the other models, 80% of the total dust flux is emitted from less than 10% of the North Africa land surface area.

3.3 Functional Relationship Between Frequency and Emission

We quantify the relationship between dust emission frequency and the emitted mass by estimating the dependency of emission on frequency using modeled annual mean emission frequency (Fig 1) and total annual emission (Fig 3). For most of the models the vast majority of the land surface area contributes very little to the total annual emission (Fig 3). To provide a better fit to the frequency and emission data we exclude grid cells having event frequencies that are less than 5% of each model's maximum North African event frequency; in the models these regions of low event frequency cumulatively contribute less than 1% to the total annual North African dust emission.

Scatterplots (Fig 4) of dust emission (E) as a function of emission frequency (f) suggest that the relationship between the two follows a power law,

$$E(f) = \alpha f^{\beta}\,, \qquad (1$$

where α and β are coefficients of the power law fit. The r-squared (r^2) and root mean squared error (RMSE) of the fit is summarized for each model in Table 2, based on a annual emission amount of 4500 Tg. All of the r^2 values are statistically significant. The r^2 values for TEGEN, CHIMERE, WRF-GOCART and CLM are all greater than or equal to 0.60 (Table 2), while that for WRF-KOK is 0.42 and for CESM if 0.27. The RMSEs for the TEGEN, CLM and two WRF models are less than 10 Tg, the RMSE for CHIMERE is approximately 12 Tg, and that for the CESM is nearly a factor of three larger than that at 28 Tg. As the fit metrics for CLM are far better than for CESM we opt to continue the study only using dust emission data from CLM and do not provide further analysis of dust from CESM (CAM).

One feature of a power law relationship is scale invariance. As annual North African dust emission is the sum over all E, if we scale emission frequency by the constant c,

$$\sum E(cf) = c^{\beta} \sum E(f),$$

or

$$\sum E(cf) \propto \sum \alpha f^{\beta}\,.$$

Thus the functional dependency of dust emission upon emission frequency scales linearly with α for different amounts of total emission, while β remains unchanged. We examine scale invariance in the relationship between dust emission and emission frequency by calculating the coefficients in (1) after scaling the 3-hourly model emission data so that the total North African dust emission is 500 to 4500 Tg, in increments of 500 Tg. All of the models except WRF-GOCART exhibit power-law behavior in that α increases linearly (Fig 5a) and β approximately remains constant (Fig 5b) as emission amount increases. The small increases in β for CHIMERE and

CLM result from the fact that the power law relationship does not hold for all values of emission frequency (Fig 3) and is valid over a range of emission frequencies.

The coefficients (1) for WRF-GOCART do not exhibit power-law behavior in that α is approximately constant (Fig 4a) and β increases nearly linearly (Fig 5b) for increasing North African dust emission. Additional analysis did not elucidate the cause of the lack of a robust power law relationship, nor show a clear alternative functional relationship between dust emission and emission frequency for WRF-GOCART. As such, we do not consider WRF-GOCART further for the purposes of estimating dust emission via the SEVIRI emission frequency data.

The multi-model mean values, which do not include WRF-GOCART, of α and β are plotted as black lines in Figure 5. Given the scale invariance of the power law relation we report the coefficients in (1) and their 95% confidence intervals for each of the models at the arbitrarily chosen total emission amount of 2500 Tg (Table 3). We also report the multi model mean values for these coefficients and their uncertainty (Table 3), which in this case is defined as the standard deviation of the model coefficients divided by the square root of one minus the number of models used to calculate the means (Wilks, 2006).

3.4 Emission Estimate from SEVIRI

Having derived empirical relationships between dust emission frequency and dust emission we next estimate a total North African mass flux based on the observational SEVIRI estimates of dust emission event frequency (Fig 1). We calculate dust emission from the SEVIRI emission frequency data via (1) using the multi-model mean coefficient values in Table 3. The main value of these SEVIRI-emission maps is to elucidate the spatial structure of emission across West Africa using observations. To emphasize this point we present the resultant SEVIRI emission data in units of percentage contribution to the total North African dust flux (Fig 6a). As such, these maps can be converted to an annual dust emission rate by multiplying the percentages by an estimate of the total annual North African dust emission. We also show the uncertainty in the SEVIRI emission estimates (Fig 6b), which is based on the uncertainty in the multimodel mean coefficients (Table 3).

Not surprisingly, the pattern of emission from SEVIRI (Fig 6a) is similar in spatial structure to the SEVIRI emission frequency data (Fig 1), except that two important hotspots emerge in the emission maps. The strongest of these hotspots is the Bodélé depression, which we define as encompassing the region of 14°-21°N and 14°-24°E (easternmost green box in Figs 6ab). In both maps the Bodélé is the region of the highest dust emission amounts (percentages) within North Africa, consistent with a number of studies suggesting as much (*e.g.*, Washington et al. 2003). The cumulative emission from the Bodélé is 64% (± 16%) of the total North Africa dust emission. Arguably the second most active region of dust emission is from a depression in the lee of the Aïr and Hoggar Mountains, which we define as encompassing the region of 16°-24°N and 2°-10°E (westernmost green box in Figs 6ab). The cumulative emission from the Aïr and Hoggar region is 13% (± 3%).

Based on the SEVIRI maps dust emission from the Bodélé and Aïr and Hoggar hotspots constitutes 77% (± 19%) of the total North African dust emission. Furthermore, from both maps the majority of all North African dust is emitted between the latitudes of 15°-20°N; the cumulative emission from the longitudinal segment spanning 15°-20°N is 82% (± 10%) of the total. Thus, according to the SEVIRI estimates, the overwhelming amount of all dust from North Africa is emitted within a 5° band of latitudes.

In comparison with emission from the models considered here (Fig 3) the SEVIRI emission estimates (Figs 6a) are most similar in spatial structure to that from the CHIMERE model. In both the SEVIRI and CHIMERE maps emission is dominated by the Bodélé. In the CHIMERE map there is a secondary maximum in emission to the west of the Bodélé that is similar is structure to the emission from the Aïr and Hoggar region. Additionally, the CHIMERE and the SEVIRI emission maps show little emission north of 25°N, whereas all of the other models exhibit substantial emission north of this latitude. However, other work has shown that the SEVIRI maps likely underestimate the frequency of emission across Northern Africa (Brindley et al. 2012). Thus the SEVIRI record may underestimate the emission frequency, which would in-turn result in a too strong an emphasis on emission equatorward of 20°N.

4. Discussion

One item not addressed thus far is the fundamental cause of the power law relationship between dust emission and dust emission frequency in the models (1). We speculate that the power law relation represents a good fit to the dust emission and emission frequency data because the sample populations (the models' distributions of emission and emission frequency) are approximately lognormal, or are characterized as having long tails.

Dust emission is though to be proportional to the cube of wind speed (*e.g.,* Marticorena and Bergametti 1995). Indeed, among the four model exhibiting a power law relationship between dust emission and emission frequency (TEGEN, WRF-KOK, CHIMERE, CLM) we find a positive and statistically significant correlation between annual mean emission and the cube of the annual mean 10m wind speed, where the correlation coefficients range from 0.49 to 0.52, with p-values all less than 0.01. In addition, histograms of the cube of annual mean 10m wind speeds for these models show that their occurrence distributions are lognormal (not shown). As such, it is not surprising that the probability distributions of annual emission are also characterized as having long tails (Fig 7a). One can also infer the lognormal probability distributions of emission in the models as the CDFs in Fig 2b increase steeply at low emission values and change little thereafter.

Similarly, the probability distributions of the TEGEN, WRF-KOK and CHIMERE models also are characterized as having long tails (Fig 7b), which is consistent with their steep rate of increase at low emission frequencies in the CDFs (Fig 2a). Although the emission frequency CDF of the CLM model does not increase steeply until scaled frequencies of 0.4 (Fig 2a), the model's probability distribution of

emission frequency does still have some characteristics consistent with a long tail (Fig 7b).

While the cubed 10m wind speed distribution from WRF-GOCART is also lognormal (not shown) the emission frequency probability distribution for this model increases very slowly at low frequencies and then peaks at high frequencies (Fig 7b), which is opposite in shape to the other four models that exhibit power law behavior. This unique and opposite characteristic of the WRF-GOCART distribution is also reflected in the emission frequency CDF (Fig 2a). We suspect this lack of a lognormal probability distribution in the WRF-GOCART emission frequency is the main reason why this model fails to show a power law relationship between emission and emission frequency.

5. Conclusions

Here we have performed a statistical analysis of North African dust emission in five models and one satellite-based data set. We firstly showed that these five models all agree that the Bodélé depression is one of the—if not the—most active dust source in West Africa, both in terms of emission amount and frequency (Figs 1 and 3). Furthermore, none of the models show dust emission south of 12°N (Fig 3). Beyond these regions, the models show widespread disagreement in the relative importance of other regions with respect to emission and frequency of events.

We examined CDFs of the frequency maps (Fig 2a). The CDFs for two models (CESM and WRF-GOCART) increased slowly for small emission frequencies and then much more rapidly at high emission event frequencies, indicating that those two models have a large number of locations that emit dust very frequently. The other four models and SEVIRI had CDFs that were more logarithmic in shape, indicating that in these models most regions infrequently emit dust, and that there are a small number of very regions with a high emission frequency. We found better agreement in CDFs of model emission; all models had a logarithmic emission CDF, indicating that emission is dominated by a small number of very active regions (Fig 2b).

We demonstrated that there is a power law relationship (1) between modeled dust emission frequency and dust emission (Fig 4) in the TEGEN, WRF-KOK, CHIMERE and CLM models (Figs 5ab). We used (1) and the coefficients in Table 3 to estimate annual mean North African dust emission based on the SEVIRI emission frequency (Figs 6ab). To the best of our knowledge this SEVIRI dust emission map represents the first observationally based estimate of the North African dust emission. Here we presented the final maps in units of percentages of total North African dust emission in order to stress that the maps are scalable to any choice of total emission.

From the observation-based map of emission we showed that the majority of dust emission from North Africa is from the Bodélé Depression and a depression in the lee of the Aïr and Hoggar Mountains (green boxes, Figs 6ab), and that 82% of all dust from North Africa is emitted between the latitudes of 15°-20°N. These results have implications for studying long-term variability of North Africa dust emission and transport in that, to first order, in order to understand the effect of the environment on regional dust emission it is particularly important to quantify

change (in surface wind speeds, soil moisture, etc.) over this narrow band of latitudes.

This study is limited in that the SEVIRI dust emission frequency record likely underestimates emission in regions frequently obscured by either clouds or dense layers of dust. Thus, while we think this new map of emission (Fig 6a) is an important step forward in generating an observation-based estimate of North African dust emission, there is a need to improve our understanding of the spatial distribution of emission across the continent. As the majority of North Africa is uninhabited, the likely only way to achieve such a goal is the deployment of an automated ground-based dust observational network.

6. Acknowledgements

The authors would like to thank the two anonymous reviewers and the associate editor for their helpful and constructive comments on an earlier version of this manuscript. This work was supported by the french Agence Nationale de la Recherche (ANR) grant ANR-10-LABX-18-01 of the national Programme Investissements d'Avenir. Funding for this work was also provided by Laboratoire d'excellence Institute Pierre Simon Laplace (L-IPSL), a grant from the "Research in Paris" programme, and National Oceanographic and Atmospheric Administration Climate Program Office grant NA11OAR4310157. S. Fiedler acknowledges the research funding by the European Research Council grant 257543. C. Zhao acknowledges support by the U.S. DOE as part of the Regional and Global Climate Modeling program. The Pacific Northwest National Laboratory is operated for DOE by Battelle Memorial Institute under contract DE-AC05-76RL01830.

7. References

Albani, S., N. M. Mahowald, A. T. Perry, R. A. Scanza, N. G. Heavens, C. S. Zender, V. Maggi, J. F. Kok, and B. L. Otto-Bliesner (2014). Improved dust representation in the Community Atmosphere Model, J. Adv. Model. Earth Syst., doi: 10.1002/2013MS000279.

Alfaro, S. C., and L. Gomes (2001), Modeling mineral aerosol production by wind erosion: Emission intensities and aerosol size distribution in source areas, J. Geophys. Res., 106, 18,075–18,084.

Albani, S., N. M. Mahowald, A. T. Perry, R. A. Scanza, N. G. Heavens, C. S. Zender, V. Maggi, J. F. Kok, and B. L. Otto-Bliesner (2013). Improved dust representation in the Community Atmosphere Model. Journal of Advances in Modeling the Earth System, submitted.

Brindley, H., Knippertz, P., Ryder, C., & Ashpole, I. (2012). A critical evaluation of the ability of the Spinning Enhanced Visible and Infrared Imager (SEVIRI) thermal infrared red-green-blue rendering to identify dust events: Theoretical analysis. *Journal of Geophysical Research: Atmospheres (1984–2012)*, *117*(D7).

Cakmur, R. V., R. L. Miller, J. Perlwitz, I. V. Geogdzhayev, P. Ginoux, D. Koch, K. E. Kohfeld, I. Tegen, and C. S. Zender (2006), Constraining the magnitude of the global dust cycle by minimizing the difference between a model and observations, J. Geophys. Res., 111, D06207, doi:10.1029/2005JD005791.

Chen, S., Huang, J., Zhao, C., Qian, Y., Leung, L. R., & Yang, B. (2013). Modeling the transport and radiative forcing of Taklimakan dust over the Tibetan Plateau: A case study in the summer of 2006. *Journal of Geophysical Research: Atmospheres*, *118*(2), 797-812.

Cowie, S. M., P. Knippertz, and J. H. Marsham (2013), Are vegetation-related roughness changes the cause of the recent decrease in dust emission from the Sahel?, Geophys. Res. Lett., 40, 1868–1872.

Creamean, J. M. et al. (2013). Dust and biological aerosols from the Sahara and Asia influence precipitation in the western US. science, 339 (6127), 1572-1578.

Das, R., A. T. Evan and D. Lawrence (2013) Contributions of long-distance dust transport to atmospheric P inputs in the Yucatan Peninsula, *Global Biogeo. Cycles*, 27, 167–175.

Dee, D. P., Uppala, S. M., Simmons, A. J., Berrisford, P., Poli, P., Kobayashi, S., ... & Vitart, F. (2011). The ERA-Interim reanalysis: Configuration and performance of the data assimilation system. *Quarterly Journal of the Royal Meteorological Society*, *137*(656), 553-597.

Doherty, O.M., Riemer, N, Hameed, S., (2014) Transport of Saharan Mineral Dust in the Boreal Summer and its Controls by the Intertropical Convergence Zone. Tellus B., In Press.

Engelstaedter, S., Tegen, I., & Washington, R. (2006). Western African dust emissions and transport. Earth-Science Reviews, 79(1), 73-100.

Engelstaedter, S., & Washington, R. (2007). Temporal controls on global dust emissions: The role of surface gustiness. *Geophysical Research Letters*, *34*(15).

Evan, A. T., J. Dunion, J. Foley, A. Heidinger and C. Velden (2006) New evidence for a relationship between Atlantic tropical cyclone activity and African dust outbreaks. Geophys. Res. Lett., 33, L19813, doi:10.1029/2006GL026408.

Evan, A. T., D. J. Vimont, R. Bennartz, J. P. Kossin and A. K. Heidinger (2009) The role of aerosols in the evolution of tropical North Atlantic Ocean temperature, Science, Vol. 324. no. 5928, pp. 778 - 781.

Evan, A. T., G. R. Foltz, D. Zhang and D. J. Vimont (2011) Influence of African dust on ocean-atmosphere variability in the tropical Atlantic, *Nature Geoscience*, 4, 762–765.

Evan, A. T., C. Flamant, S. Fiedler, O. Doherty (2014) An analysis of aeolian dust in climate models. *Geophys. Res. Lett.*, doi: 10.1002/2014GL060545, *in press*.

Fiedler, S., K. Schepanski, B. Heinold, P. Knippertz, and I. Tegen (2013a), Climatology of nocturnal low-level jets over Western Africa and implications for modeling mineral dust emission, J. Geophys. Res. Atmos., 118, 6100–6121.

Fiedler, S., K. Schepanski, P. Knippertz, B. Heinold, and I. Tegen (2014), How important are cyclones for emitting mineral dust aerosol in Western Africa?, *Atmos. Chem. Phys.*, 14, 8983-9000, doi:10.5194/acp-14-8983-2014.

Ginoux, P., Chin, M., Tegen, I., Prospero, J. M., Holben, B., Dubovik, O., & Lin, S. J. (2001). Sources and distributions of dust aerosols simulated with the GOCART model. *Journal of Geophysical Research: Atmospheres (1984–2012)*, *106*(D17), 20255-20273.

Grell, G. A., Peckham, S. E., Schmitz, R., McKeen, S. A., Frost, G., Skamarock, W. C., & Eder, B. (2005). Fully coupled "online" chemistry within the WRF model. *Atmospheric Environment*, *39*(37), 6957-6975.

Hurrell, James W., and Coauthors, 2013: The Community Earth System Model: A Framework for Collaborative Research. *Bull. Amer. Meteor. Soc.*, **94**, 1339–1360.

Johnson, B. T., M. E. Brooks, D. Walters, S. Woodward, S. Christopher, and K. Schepanski (2011), Assessment of the Met Office dust forecast model using

observations from the GERBILS campaign, *Quart. J. Roy. Met. Soc*., 137 (658), 1131-1148, doi:10.1002/qj.736.

Kalenderski, S., Stenchikov, G., & Zhao, C. (2012). Modeling a typical winter-time dust event over the Arabian Peninsula and the Red Sea. *Atmos. Chem. Phys.*, *12*(10).

Knippertz, P., & Todd, M. C. (2012). Mineral dust aerosols over the Sahara: Meteorological controls on emission and transport and implications for modeling. *Rev. Geophys.*, *50*(1).

Kocha, C., P. Tulet , J.-P. Lafore, C. Flamant, 2013: The importance of the diurnal cycle of aerosol optical thickness in West Africa, *Geophys. Res. Letter*, **40(4),** 785-790, doi:10.1002/grl.50143

Kok, J. F. (2011). A scaling theory for the size distribution of emitted dust aerosols suggests climate models underestimate the size of the global dust cycle. *Proceedings of the National Academy of Sciences*, *108*(3), 1016-1021.

Kok, J. F., Mahowald, N. M., Albani, S., Fratini, G., Gillies, J. A., Ishizuka, M., Leys, J. F., Mikami, M., Park, M.-S., Park, S.-U., Van Pelt, R. S., Ward, D. S., and Zobeck, T. M. (2014). An improved dust emission model with insights into the global dust cycle's climate sensitivity. *Atmospheric Chemistry & Physics*, *14*(5).

Laurent, B., I. Tegen, B. Heinold, K. Schepanski, B. Weinzierl, and M. Esselborn (2010), A model study of Saharan dust emissions and distributions during the SAMUM-1 campaign, J. Geophys. Res., 115, D21210.

Mahowald, N. M., Yoshioka, M., Collins, W. D., Conley, A. J., Fillmore, D. W., & Coleman, D. B. (2006). Climate response and radiative forcing from mineral aerosols during the last glacial maximum, pre-industrial, current and doubled-carbon dioxide climates. *Geophysical Research Letters*, *33*(20).

Mahowald, N. M.,S. Kloster, S. Engelstaedter, J. Keith Moore, S. Mukhopadhyay, Joseph R. McConnell, S. Albani Observed 20th century desert dust variability: impact on climate and biogeochemistry, *Atmos. Chem. Phys.*, 10, 10875-10893, doi:10.5194/acp-10-10875-2010, 2010.

Marticorena, B., and G Bergametti (1995), Modeling the atmospheric dust cycle: 1. Design of a soil-derived dust emission scheme, J. Geophys. Res., 100(D8), 16,415–16,430.

Menut L., C.Schmechtig and B.Marticorena, 2005, Sensitivity of the sandblasting fluxes calculations to the soil size distribution accuracy, Journal of Atmospheric and Oceanic Technology, 22, No. 12, pages 1875-1884.

Menut L., C.Perez Garcia-Pando, K.Haustein, B.Bessagnet, C.Prigent and S.Alfaro, 2013, Relative impact of roughness and soil texture on mineral dust emission fluxes

modeling, Journal of Geophysical Research Atmospheres, 118, 6505-6520, doi:10.1002/jgrd.50313

Okin, G. S., A.R. Baker, I. Tegen, N. M. Mahowald, F. J. Dentener, R. A. Duce and J. N. Galloway (2011), Impacts of atmospheric nutrient deposition on marine productivity: Roles of nitrogen, phosphorus, and iron, *Global Biogeochem. Cycles*, 25, GB2022, doi:10.1029/2010GB003858.

Prospero, J. M., Ginoux, P., Torres, O., Nicholson, S. E., & Gill, T. E. (2002). Environmental characterization of global sources of atmospheric soil dust derived from the Nimbus 7 TOMS absorbing aerosol product, rev. In *Reviews of Geophysics*.

Ridley, D. A., Heald, C. L., and Prospero, J. M.: What controls the recent changes in African mineral dust aerosol across the Atlantic?, *Atmos. Chem. Phys.*, 14, 5735-5747, doi:10.5194/acp-14-5735-2014, 2014.

Schepanski, K., Tegen, I., Laurent, B., Heinold, B., & Macke, A. (2007). A new Saharan dust source activation frequency map derived from MSG-SEVIRI IR-channels. *Geophysical Research Letters*, *34*(18).

Schepanski, K., Tegen, I., Todd, M.C., Heinold, B., Bönisch, G., Laurent, B., & Macke, A. (2009). Meteorological processes forcing Saharan dust emission inferred from MSG-SEVIRI observations of sub-daily source activation and numerical models, J. Geophys. Res., 114, D10201, doi:10.1029/2008JD010325.

Schepanski, K., Tegen, I., & Macke, A. (2012). Comparison of satellite based observations of Saharan dust source areas. *Remote Sensing of Environment*, *123*, 90-97.

Skamarock, W. C., & Klemp, J. B. (2008). A time-split nonhydrostatic atmospheric model for weather research and forecasting applications. *Journal of Computational Physics*, *227*(7), 3465-3485.

Tegen, I., S. Harrison, K. Kohfeld, I. Prentice, M. Coe, and m. Heimann (2002), Impact of vegetation and preferential source areas on global dust aerosols: Results from a model study, *J. Geophys. Res.*, **107**(D21), 4576.

Tegen, I., and R. Miller (1998), A general circulation model study on the interannual variability of soil dust aerosol, J. Geophys. Res., 103(D20), 25975–25995, doi:10.1029/98JD02345.

Tegen, I., Schepanski, K., & Heinold, B. (2013), Comparing two years of Saharan dust source activation obtained by regional modelling and satellite observations. *Atmospheric Chemistry and Physics*, *13*(5), 2381-2390.

Todd, M. C., et al. (2008), Quantifying uncertainty in estimates of mineral dust flux: An intercomparison of model performance over the Bodélé Depression, northern Chad, *J. Geophys. Res.*, 113, D24107, doi:10.1029/2008JD010476.

Washington, R. W., M. C. Todd, N. Middleton, and A. S. Goudie (2003), Dust-storm source areas determined by the Total Ozone Monitoring Spectrometer and surface observations, *Ann. Assoc. Am. Geogr.*, 93, 297–313, doi:10.1111/1467-8306.9302003.

Zender, C. S., Bian, H., & Newman, D. (2003). Mineral Dust Entrainment and Deposition (DEAD) model: Description and 1990s dust climatology. *Journal of Geophysical Research: Atmospheres (1984–2012)*, *108*(D14).

Zhao, C., Liu, X., Leung, L. R., Johnson, B., McFarlane, S. A., Gustafson Jr, W. I., ... & Easter, R. (2010). The spatial distribution of mineral dust and its shortwave radiative forcing over Western Africa: modeling sensitivities to dust emissions and aerosol size treatments. *Atmospheric Chemistry and Physics*, *10*(18), 8821-8838.

Zhao, C., Liu, X., Leung, L. R. & Hagos, S. (2011). Radiative impact of mineral dust on monsoon precipitation variability over West Africa. *Atmospheric Chemistry and Physics*, *11*(5), 1879-1893.

Zhao, C., Liu, X., Leung, L. R. (2012). Impact of the Desert dust on the summer monsoon system over Southwestern North America. *Atmospheric Chemistry and Physics*, *12*(8), 3717-3731.

Zhao, C., S Chen, LYR Leung, Y Qian, J Kok, RA Zaveri, and J Huang (2013). Uncertainty in Modeling Dust Mass Balance and Radiative Forcing from Size Parameterization. *Atmospheric Chemistry and Physics* 13, 10733-10753.

8. Tables

Model	Dust emission	Boundaries	Horiz. Resolution	Output
TEGEN	Offline, 3 bins (Tegen et al. 2002)	ERA-Interim forecasts (Dee et al. 2011)	Western Africa 1x1 degree res	3-Hourly
WRF-GOCART	Online, 3 mode (Zhao et al. 2013)	Forced everywhere with NCAR/NCEP reanalysis	60°S to 70°N and all longitudes 1x1 degree res	3-Hourly
WRF-Kok	Online, 3 mode (Kok et al. 2014)		60°S to 70°N and all longitudes 1x1 degree res	3-Hourly
CESM	Online, 3 bins (Mahowald et al. 2006)	N/A	Global 0.94° x 1.24° res	30-Minute
CHIMERE	Online, 9 bins (0.039 to 40 um), saltation & sandblasting, (Menut et al., 2013)	N/A	Global 1x1 degree res	Hourly

Table 1: Overview of model characteristics. Shown here are models' dust emission scheme types and number of bins, meteorological forcing at model boundaries, horizontal resolution, and model output data time resolution. All dust output fields are instantaneous.

Model	r^2	RMSE (Tg)
Tegen	0.68	3.7
WRF-Kok	0.42	6.4
CHIMERE	0.64	11.9
WRF-GOCART	0.60	2.3
CESM	0.27	27.82
CLM	0.64	5.1

Table 2: Emission and emission frequency fit statistics. Shown are the r-squared (r^2) and root mean squared error (RMSE) for each model from power law fit of dust emission as a function of emission event frequency (1). All r^2 values are statistically significant at the 95% level.

Model	α	β
TEGEN	82.3±8.0	1.30±0.05
WRF-KOK	227.7±57.2	1.92±0.14
CHIMERE	107.7±13.3	3.95±0.35
CLM	74.2±6.6	3.16±0.14
Mean	**123.0±41.1**	**2.58±0.69**

Table 3: Power law coefficients. Shown are the coefficients and standard error from the power law fit of the emission and emission frequency data (Eqns 1, 2). These values represent the mean coefficient values from Figure 5 at a total North Africa emission amount of 2500 Tg. The bold numbers represent the multi-model mean values that are used to estimate dust emission from SEVIRI. The uncertainty ranges for the multi-model mean values are defined as the standard deviation of the models' regression coefficients divided by the square root of one minus the number of models (the standard error on the mean value estimates).

9. Figures

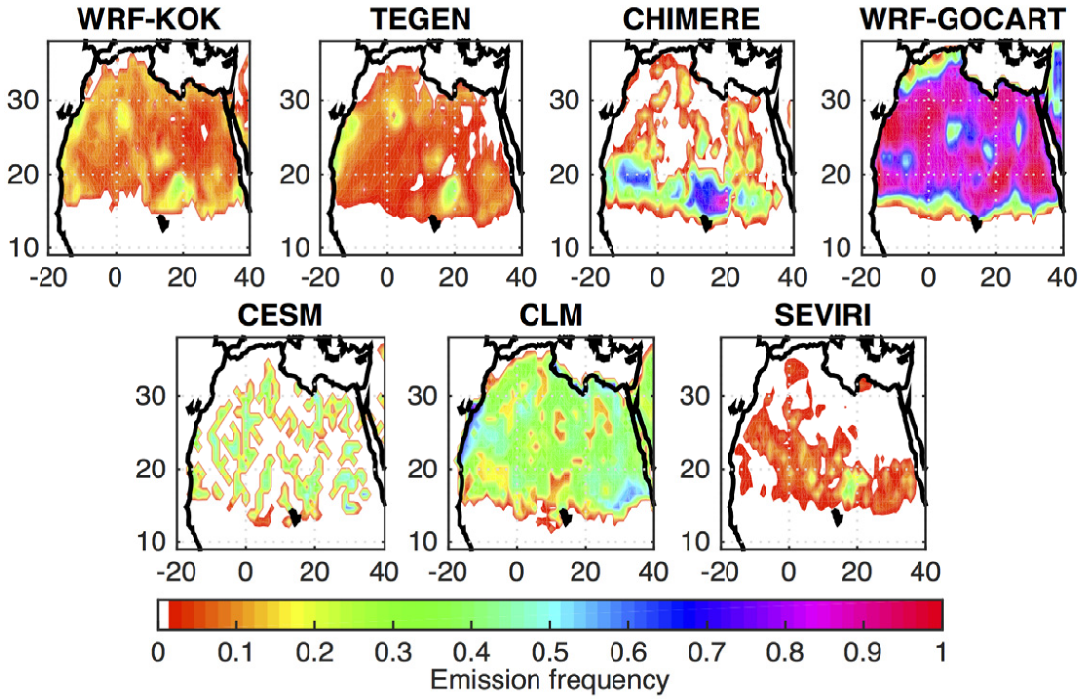

Figure 1. Emission frequency from models and satellite imagery. Shown are maps of dust emission event frequency calculated from 3-hourly emission from the six models analyzed here and the 3-hourly satellite imagery.

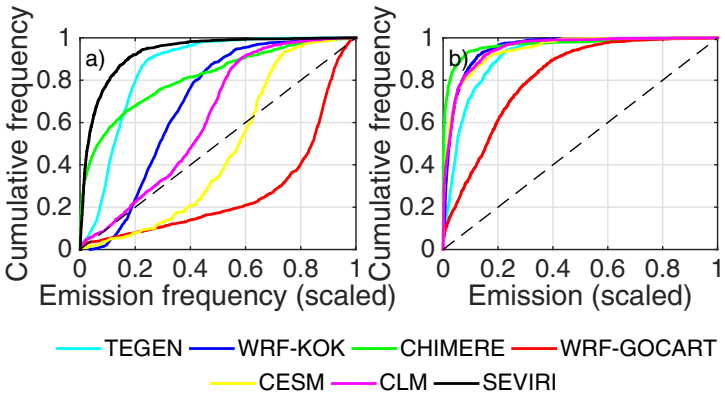

Figure 2. Dust emission frequency cumulative distribution functions and sensitivity of emission to frequency. Plotted (2a) are cumulative distribution functions (CDFs) for the annual mean emission frequencies from models and satellite data (Figure 1). Here all data has been linearly scaled to have a maximum frequency of 1 to facilitate model intercomparison. Also shown (2b) are the CDFs of emission for the six models, again where emission has been scaled to a maximum value of one. In both plots the identify line (black dashed) is plotted for reference.

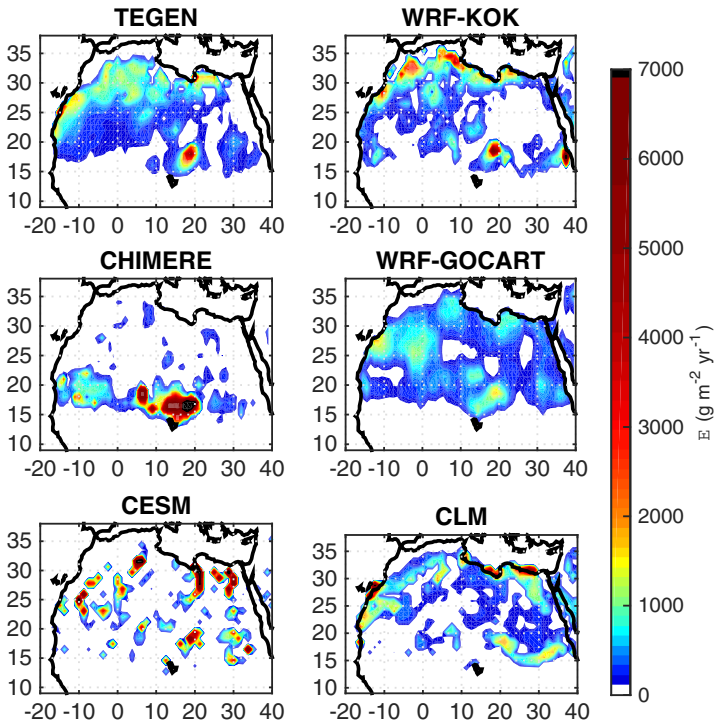

Figure 3. Annual mean emission from models and satellite imagery. Shown are maps of emission (g m^{-2} per year) calculated from the 3-hourly output of the six models in Figure 1.

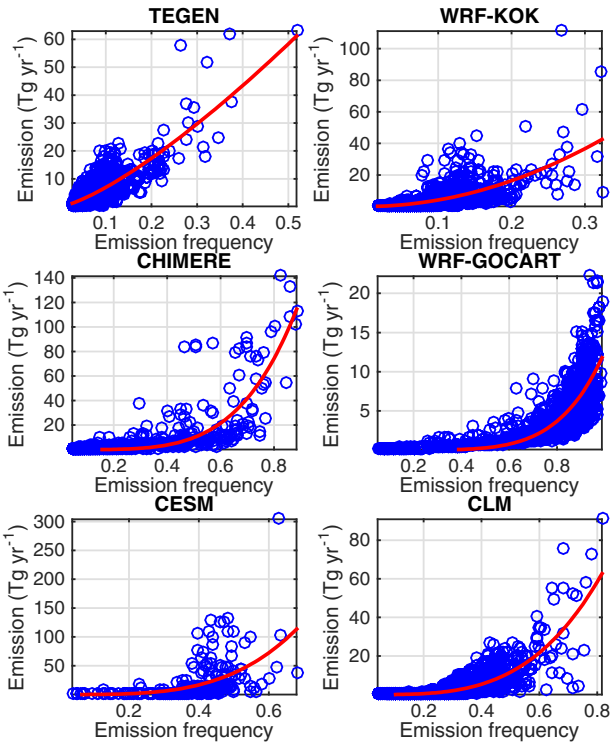

Figure 4. Plots of modeled emission frequency and emitted mass. Shown are scatterplots of annual mean dust emission (ordinate) and emission event frequency for the six models examined here (blue circles). Also shown are the power law fits (1) to the data (red lines), based on an annual emission amount of 4500 Tg. Table 2 contains a summary of the fit statistics.

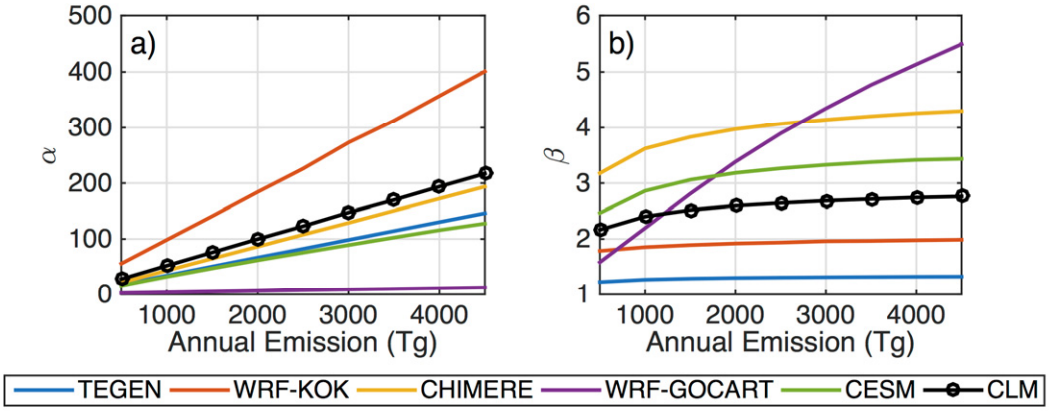

Figure 5. Power law coefficients. Shown are values of the α (5a) and β (5b) coefficients (1) from from a least-squares fit of the dust emission and emission frequency data for five models (ordinate). The coefficients are calculated for different emission amounts (indicated in the absiscca). The black line indicates the multi-model mean values, which is not calculated using WRF-GOCART. The coefficient values at 2500 Tg is indicated in Table 3.

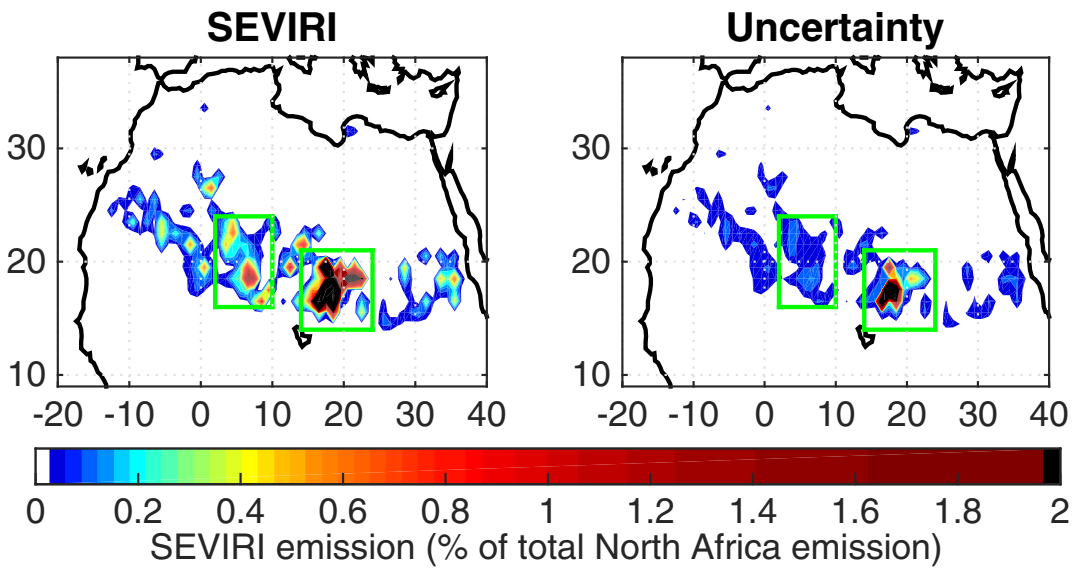

Figure 6. Estimate of annual emission rates from SEVIRI. Shown are SEVIRI-derived maps of annual mean dust emission from (1) using the multimodel mean coefficients in Table 3 (left) and the uncertainty in the estimate based on the standard error on the coefficients (right). The data is in units of % of annual North Africa dust emission. The green boxes outline the major dust hotspots of the Bodélé Depression (easternmost box) and a depression in the lee of the Aïr and Hoggar Mountains (westernmost box).

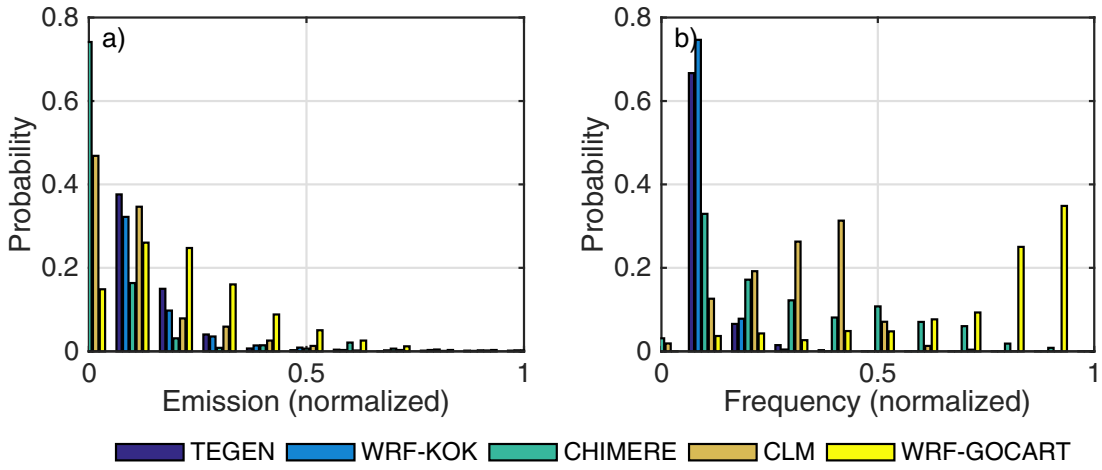

Figure 7. Probability distributions. Shown are the probability distributions of annual dust emission (7a) and emission frequency (7b) for five models.